10-5-1988

Inulin-^{125}I-Tyramine, an Improved Residualizing Label for Studies on Sites of Catabolism of Circulating Proteins

Janet L. Maxwell

John W. Baynes
University of South Carolina - Columbia, john.baynes@sc.edu

Suzanne R. Thorpe

Publication Info

Published in *Journal of Biological Chemistry*, Volume 263, Issue 28, 1988, pages 14122-14127.
This research was originally published in the Journal of Biological Chemistry. Maxwell JL, Baynes JW, Thorpe SR. Inulin-125 I-Tyramine, an Improved Residualizing Label for Studies on Sites of Catabolism of Circulating Proteins. *Journal of Biological Chemistry*. 1988; 263:14122-14127. © the American Society for Biochemistry and Molecular Biology.

THE JOURNAL OF BIOLOGICAL CHEMISTRY
Vol. 263, No. 28, Issue of October 5, pp. 14122-14127, 1988
Printed in U.S.A.

Inulin-^{125}I-Tyramine, an Improved Residualizing Label for Studies on Sites of Catabolism of Circulating Proteins*

(Received for publication, February 4, 1988)

Janet L. Maxwell‡, John W. Baynes‡§, and Suzanne R. Thorpe‡¶

From the ‡Department of Chemistry and the §School of Medicine, University of South Carolina, Columbia, South Carolina 29208

Residualizing labels for protein, such as dilactitol-^{125}I-tyramine (^{125}I-DLT) and cellobiitol-^{125}I-tyramine, have been used to identify the tissue and cellular sites of catabolism of long-lived plasma proteins, such as albumin, immunoglobulins, and lipoproteins. The radioactive degradation products formed from labeled proteins are relatively large, hydrophilic, resistant to lysosomal hydrolases, and accumulate in lysosomes in the cells involved in degradation of the carrier protein. However, the gradual loss of the catabolites from cells ($t_{1/2}$ ~ 2 days) has limited the usefulness of residualizing labels in studies on longer lived proteins. We describe here a higher molecular weight (M_r ~ 5000), more efficient residualizing glycoconjugate label, inulin-^{125}I-tyramine (^{125}I-InTn). Attachment of ^{125}I-InTn had no effect on the plasma half-life or tissue sites of catabolism of asialofetuin, fetuin, or rat serum albumin in the rat. The half-life for hepatic retention of degradation products from ^{125}I-InTn-labeled asialofetuin was 5 days, compared to 2.3 days for ^{125}I-DLT-labeled asialofetuin. The whole body half-lives for radioactivity from ^{125}I-InTn-, ^{125}I-DLT-, and ^{125}I-labeled rat serum albumin were 7.5, 4.3, and 2.2 days, respectively. The tissue distribution of degradation products from ^{125}I-InTn-labeled proteins agreed with results of previous studies using ^{125}I-DLT, except that a greater fraction of total degradation products was recovered in tissues. Kinetic analyses indicated that the average half-life for retention of ^{125}I-InTn degradation products in tissues is ~5 days and suggested that *in vivo* there are both slow and rapid routes for release of degradation products from cells. Overall, these experiments indicate that ^{125}I-InTn should provide greater sensitivity and more accurate quantitative information on the sites of catabolism of long-lived circulating proteins *in vivo*.

Residualizing labels are biologically inert radioactive tags used for studies on the sites of protein catabolism *in vivo*. These labels are designed to yield limit, hydrophilic degradation products of a sufficient size that they are retained in lysosomes following catabolism of the carrier protein. The sites of degradation of the labeled protein may then be determined either by measuring acid-soluble radioactivity in various tissues and cells or by autoradiography. Residualizing labels, such as [^{3}H]raffinose (2), dilactitol-^{125}I-tyramine (^{125}I-DLT)[1] (3), and cellobiitol-^{125}I-tyramine (4), have been used to identify the tissue and cellular sites of catabolism of plasma proteins, such as albumin (5–7), lipoproteins (4, 8), and immunoglobulins (9), and are also being increasingly used in studies on the uptake and catabolism of proteins by cells in culture (8, 10). One of the limitations of the use of these labels, however, is that whereas their rate of loss from cells is slow ($t_{1/2}$ ~ 2 days for ^{125}I-DLT in rat tissues), the rates of catabolism of plasma proteins are often equally slow or slower. Thus, a substantial fraction of degradation products is lost from tissues by the time significant amounts of the protein have been catabolized. Under these circumstances, it is not possible to assess rigorously the quantitative role of various tissues in catabolism of a protein since the distribution of degradation products in the body could be biased by differences in the rate of loss of the label from various cell types.

Because of the limited residualization of tetrasaccharide derivatives of tyramine and the fact that residualization is improved with increasing saccharide content or molecular weight of the label (3), we set out to design a higher molecular weight oligosaccharide derivative of tyramine, with the expectation that this label would be retained more efficiently in cells. We describe here the biological properties of inulin-^{125}I-tyramine (^{125}I-InTn), a residualizing glycoconjugate label derived from the inert fructan polymer inulin (M_r ~ 5000). The retention of protein degradation products containing the ^{125}I-InTn label results from both their size and the absence of lysosomal fructofuranosidase activity (11). As shown below, ^{125}I-InTn, the largest residualizing label for protein described thus far, has negligible effects on the kinetics or tissue sites of plasma protein catabolism and is retained in lysosomes more efficiently than is ^{125}I-DLT. The data indicate that ^{125}I-InTn should be widely applicable in studies on the catabolism of long-lived circulating proteins.

EXPERIMENTAL PROCEDURES AND RESULTS[2]

The chemistry of synthesis and coupling of ^{125}I-InTn to protein is outlined in Fig. 1 and described in detail under "Experimental Procedures." Also described in the Miniprint are a series of preliminary experiments validating the usefulness of InTn in studies on catabolism of circulating proteins such as asialofetuin and fetuin. The effectiveness of InTn as a residualizing label is clearly illustrated in Fig. 5, which shows both the plasma and whole body kinetics of clearance of ^{125}I-, ^{125}I-DLT-, and ^{125}I-InTn-labeled RSA. Notably, as

* This work was supported by National Institutes of Health Research Grant DK 25373. A preliminary report of this work has been presented (1). The costs of publication of this article were defrayed in part by the payment of page charges. This article must therefore be hereby marked "*advertisement*" in accordance with 18 U.S.C. Section 1734 solely to indicate this fact.

¶ To whom correspondence should be addressed.

[1] The abbreviations used are: ^{125}I-DLT, dilactitol-^{125}I-tyramine; ^{125}I-InTN, inulin-^{125}I-tyramine; RSA, rat serum albumin; *I, ^{125}I.

[2] Portions of this paper (including "Experimental Procedures," part of "Results," Figs. 2–4 and 6, and Tables I–III) are presented in miniprint at the end of this paper. Miniprint is easily read with the aid of a standard magnifying glass. Full size photocopies are included in the microfilm edition of the Journal that is available from Waverly Press.

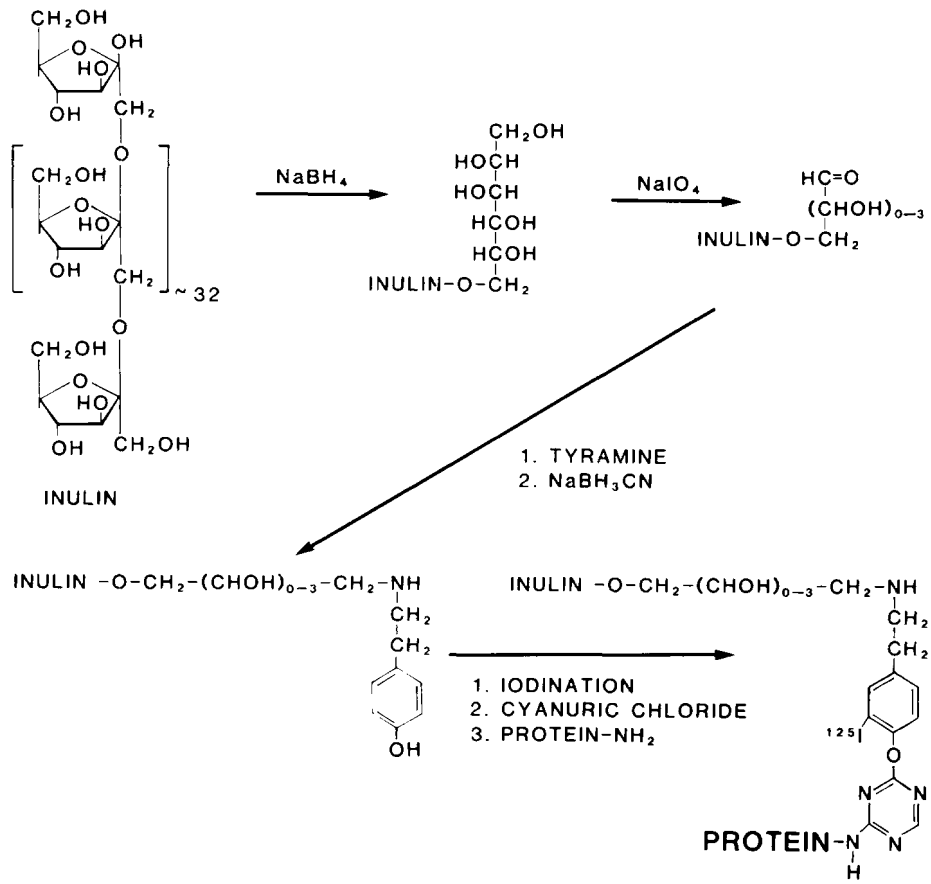

FIG. 1. **Reaction scheme for synthesis of ^{125}I-InTn and its coupling to protein.** Inulin is reduced with $NaBH_4$, and the terminal alditol is oxidized with a limiting amount of periodate to generate an aldehyde. Tyramine is coupled to inulin aldehyde by reductive amination using $NaBH_3CN$, yielding InTn. InTn is then labeled with radioactive iodine using IODO-GEN and coupled to protein using cyanuric chloride.

with asialofetuin and fetuin, the plasma half-life of RSA was unaffected by the attachment of InTn. The ^{125}I-InTn degradation products also residualized more efficiently, with a whole body half-life of about 7.5 days, compared to 4–5 days for ^{125}I-DLT (Fig. 5 and Ref. 7). The tissue distribution of radioactivity at 4 days after injection of ^{125}I-InTn-labeled RSA, shown in Table II, confirms previous evidence using ^{125}I-DLT-labeled RSA that catabolism of RSA takes place primarily in muscle and skin (7). However, in these experiments, a significantly greater fraction of total degradation products was retained in the body. Thus, the circulating half-life of this preparation of ^{125}I-InTn-labeled RSA was 1.8 days, *i.e.* 79% catabolism at 4 days; the loss of 27% of radioactivity from the body by 4 days indicates that about 66% (27:79) of the theoretical yield of ^{125}I-InTn-labeled RSA degradation products was recovered, compared to 45% for ^{125}I-DLT-labeled RSA (7). Overall, with all three proteins studied, the ^{125}I-InTn label yielded results consistent with previous studies using other labels, but with substantially improved retention of degradation products in the body.

Kinetic Modeling of Plasma Protein Catabolism—As a first step toward understanding the biological behavior of residualizing labels, we have attempted to develop kinetic models for quantitative comparison of the rates of loss of the various labels from tissues. For this purpose, we have used SCoP and SCoPfit programs, which are simulation control and optimization programs developed for the IBM-PC/AT computer by the National Biomedical Simulation Resource at Duke University (Durham, NC). SCoP generates a graphical simulation of a kinetic process, given a series of differential equations (the kinetic model) and specified kinetic constants. The SCoPfit program accepts actual experimental data and, using the SCoP model, develops kinetic constants to optimize the fit of experimental data to the model. For the purpose of illustrating the results of calculations, experimental data from Fig. 5 (*lower*) are replotted in Fig. 7, showing the kinetics of whole body release of degradation products from ^{125}I-DLT-labeled RSA (Fig. 7, *upper*) and ^{125}I-InTn-labeled RSA (Fig. 7, *lower*). The various lines drawn on the graph represent different fits to the data using the SCoP or SCoPfit program with various models and assumptions, as described in detail in the Miniprint. In summary, the *dotted lines* are derived from the SCoP program using the three-compartment model described in Fig. 6 and assuming that RSA degradation products leak from all tissues at the same rate at which asialofetuin degradation products leak from liver. Because of the poor fit to the experimental data, SCoPfit was used with the same model to optimize the kinetic constants and to improve the fit to the data. However, this SCoPfit optimization (*dashed lines*) was also unsatisfactory, and systematic error was apparent, suggesting that the model was inappropriate. Since recent work by Buktenica *et al.* (30) indicated that degradation products were routed through both slow and fast release compartments in cells *in vitro*, the three-compartment model was revised to allow for a fraction of degradation products to be released rapidly from cells *in vivo*. The *solid lines* in Fig. 7 (*upper* and *lower*) are the results of SCoPfit optimizations to this revised model and yield good and consistent fits to the experimental data. The development, mathematical description and assumptions, and the kinetic constants obtained with the various models are described in detail in the Miniprint.

DISCUSSION

The need for residualizing labels which are more completely retained in tissues has been apparent since the earliest experiments using this technology to identify the sites of plasma

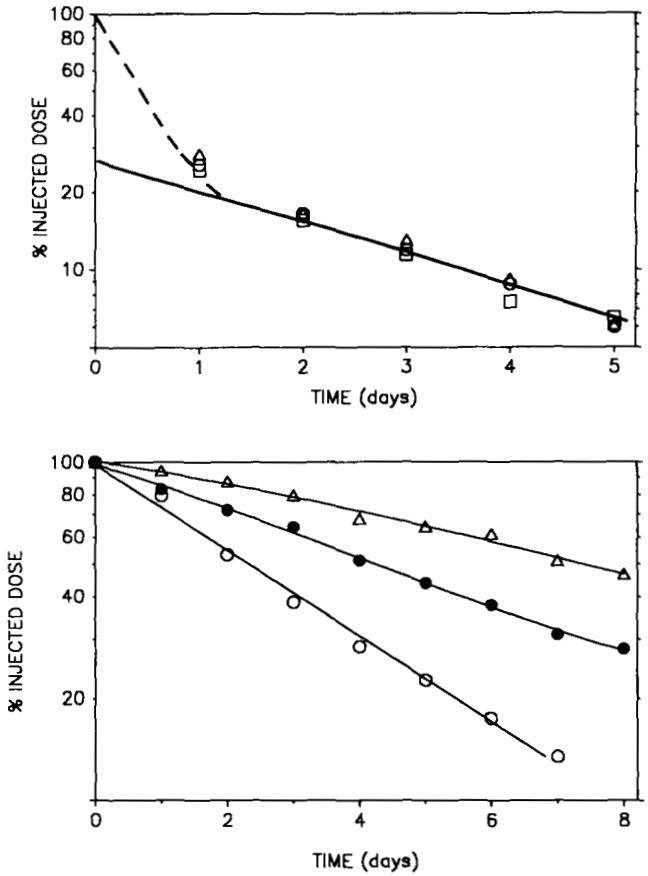

FIG. 5. **Kinetics of plasma and whole body clearance of radioactivity from RSA labeled with ^{125}I, ^{125}I-DLT, or ^{125}I-InTn.** *Upper*, kinetics of clearance of RSA from the circulation. Animals were injected with 10×10^6 cpm (50–100 μg) of protein labeled with ^{125}I (○), ^{125}I-DLT (□), or ^{125}I-InTn (△). *Lower*, kinetics of whole body clearance of RSA. Animals were injected with 2.5×10^6 cpm of protein labeled with ^{125}I (○), ^{125}I-DLT (●), or ^{125}I-InTn (△).

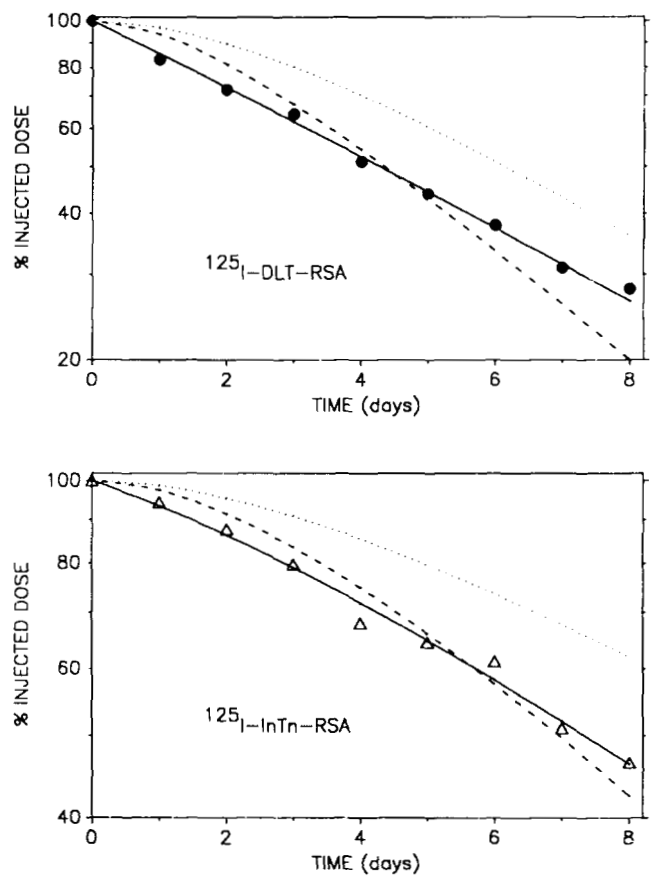

FIG. 7. **Results of kinetic modeling to estimate rate of leakage of various labels from cells.** The data are replotted from Fig. 5, *bottom*. The fitted lines are derived from equations described in text, and kinetic constants are listed in Table III.

protein catabolism. Because of the gradual loss of degradation products from tissues, it has been necessary to terminate experiments at times when only a fraction of the protein has been catabolized and then to apply corrections for intact protein remaining in tissues, for example, by acid precipitation of the intact protein (3, 7) or by injection of a second, nonresidualizing tracer to estimate the amount of intact protein in the tissue (31). These manipulations are not only inconvenient, but they also ultimately affect the precision of estimates of protein degradation in tissues. Our previous work had revealed a relationship between the number of carbohydrate units in the label and its efficiency of residualization (3), so that the synthesis of a larger glycoconjugate label seemed a reasonable route for improving residualization. There are obvious limits to this approach, however, since at some point the size or properties of the label itself will affect the mechanisms and sites of catabolism of the carrier protein.

An inulin derivative was chosen as a reasonably sized target since the resulting molecular weight of the label would be, at most, about 10% of the mass of the smallest plasma protein. The synthesis of InTn was straightforward, and its iodination and coupling to protein proceeded with good efficiency, 30 and 70%, respectively. Thus, only nanomolar quantities are required to label proteins with high specific radioactivity. The inertness of underivatized inulin in the coupling reaction is also convenient because this inulin serves as a carrier to decrease losses during handling, does not appear to interfere with labeling of the protein, and is readily separated from labeled protein by gel exclusion chromatography. In all of the experiments described here, the average substitution of protein was limited to <1 mol of ^{125}I-InTn/mol of protein in order to decrease the probability of multiple derivatization of carrier proteins. The addition of 1 mol of ^{126}I-InTn/mol of protein had no detectable effect on the kinetics, mechanisms, or sites of catabolism of asialofetuin, fetuin, or RSA. This result is consistent with recent hypotheses on the regulation of protein catabolism. Thus, the kinetics of protein catabolism appear to be determined by genetically encoded molecular features of the protein molecule, such as the amino-terminal amino acid or a sequence or array of amino acids in the primary or tertiary structure of the protein, rather than by bulk physical characteristics such as hydrophobicity, subunit molecular weight, or isoelectric point (32).

The size of the radioactive products isolated from urine using the [^{3}H]raffinose (2), ^{125}I-DLT (3), or ^{125}I-InTN labels indicates that residualizing labels are excreted from the body largely in intact form. Thus, following catabolism of the carrier protein, the labeled degradation products appear to be released from cells by the process of exocytosis or regurgitation, rather than by deiodination or eventual hydrolysis to lower molecular weight products. The difference in whole body half-life of radioactivity from asialofetuin labeled with raffinose, DLT, InTn, and other labels (3) indicates that the structure of the label affects its rate of release from cells. In addition, however, kinetic analysis indicates that there are also differences in the routes of transport of these indigestible

compounds within the cell. Thus, whereas some residualization was observed with all of the labels, there was a fraction of these labels rapidly released from the body so that a significant lag phase in whole body clearance was not observed (Figs. 4 and 5, *lower*). Based on kinetic analysis, we have concluded that degradation products may be partitioned between slow and fast release compartments within the cell and that routing of the partially degraded protein or labeled degradation products to the fast release compartment may be an important factor limiting the long-term retention of catabolites in the body. Our model makes no statement regarding the nature of the fast release compartment, although it is likely to be an early endocytic compartment, either prelysosomal or in equilibrium with the lysosomal compartment. Whereas larger residualizing labels could theoretically prove more efficient, there is greater risk that they will affect the catabolism of the carrier protein. For most purposes, the InTn label should be suitable, for example, in studies on the catabolism of IgGs, which are among the longest lived circulating proteins ($t_{½}$ = 3–5 days in the rat).

Acknowledgment—We thank Thomas G. Huggins (Department of Chemistry, University of South Carolina) for assistance in using the SCoP and SCoPfit programs.

REFERENCES

1. Maxwell, J. L., Baynes, J. W., and Thorpe, S. R. (1986) *Fed. Proc.* **45,** 1540
2. Van Zile, J., Henderson, L. A., Baynes, J. W., and Thorpe, S. R. (1979) *J. Biol. Chem.* **254,** 3547–3553
3. Strobel, J. L., Baynes, J. W., and Thorpe, S. R. (1985) *Arch. Biochem. Biophys.* **240,** 635–645
4. Pittman, R. C., and Taylor, C. A., Jr. (1986) *Methods Enzymol.* **129,** 612–628
5. Baynes, J. W., and Thorpe, S. R. (1981) *Arch. Biochem. Biophys.* **206,** 372–379
6. Yedgar, S., Carew, T. E., Pittman, R. C., Beltz, W. F., and Steinberg, D. (1983) *Am. J. Physiol.* **244,** E101–E107
7. Strobel, J. L., Cady, S. G., Borg, T. K., Terracio, L., Baynes, J. W., and Thorpe, S. R. (1986) *J. Biol. Chem.* **261,** 7989–7994
8. Daugherty, A., Thorpe, S. R., Lange, L. G., Sobel, B. E., and Schonfeld, G. (1985) *J. Biol. Chem.* **260,** 14564–14570
9. Henderson, L. A., Baynes, J. W., and Thorpe, S. R. (1982) *Arch. Biochem. Biophys.* **215,** 1–11
10. Maxwell, J. M., Baynes, J. W., and Thorpe, S. R. (1987) in *The Pharmacology and Toxicology of Proteins* (Winkelhake, J. L., and Holcenberg, J. S., eds) pp. 59–72, Alan R. Liss, Inc., New York
11. Wattiaux, R. (1977) in *Mammalian Cell Membranes* (Jamison, G. A., and Robinson D. M., eds.) Vol. 2, pp. 165–184, Butterworth & Co., Ltd., London
12. Dulbecco, R., and Vogt, M. S. (1954) *J. Exp. Med.* **98,** 167–173
13. Laemmli, U. K. (1970) *Nature* **227,** 680–685
14. Aspinall, G. O. (1970) *Polysaccharides*, pp. 80–83, Pergamon Press, London
15. McFeeters, R. F. (1980) *Anal. Biochem.* **103,** 302–306
16. Spiro, R. G. (1966) *Methods Enzymol.* **8,** 3–25
17. Raja, R. H., LeBoeuf, R. D., Stone, G. W., and Weigel, P. H. (1984) *Anal. Biochem.* **139,** 168–177
18. Avigad, G. (1969) *Carbohydr. Res.* **11,** 113–118
19. Gregoriadis, G., and Sourkes, T. L. (1967) *Can. J. Biochem.* **45,** 1841–1848
20. Deleted in proof
21. Deleted in proof
22. Smith, N. L., and Lenhoff, H. M. (1974) *Anal. Biochem.* **61,** 392–415
23. Ashwell, G., and Harford, J. (1982) *Annu. Rev. Biochem.* **51,** 531–554
24. Baynes, J. A., Van Zile, J., Henderson, L. A., and Thorpe, S. R. (1980) *Birth Defects Orig. Art. Ser.* **16,** 103–113
25. Murtiashaw, M. H., Baynes, J. W., and Thorpe, S. R. (1983) *Arch. Biochem. Biophys.* **225,** 256–262
26. Carew, T. E., Pittman, R. C., Marchand, E. R., and Steinberg, D. (1984) **4,** 214–224
27. Cohn, Z. A., and Ehrenreich, B. A. (1969) *J. Exp. Med.* **129,** 201–225
28. Besterman, J. M., Airhart, J. A., Woodworth, R. C. and Low, R. B. (1981) *J. Cell. Biol.* **91,** 716–727
29. Hoppe, C. A., and Lee, Y. C. (1984) *Biochemistry* **23,** 1723–1730
30. Buktenica, S., Olenick, S. J., Salgia, R., and Frankfater, A. (1987) *J. Biol. Chem.* **262,** 9469–9476
31. Pittman, R. C., Carew, T. E., Glass, C. K., Green, S. R., Taylor, C. A., and Attie, A. D. (1983) *Biochem. J.* **212,** 791–800
32. Rechsteiner, M., Rogers, S., and Rote, K. (1987) *Trends Biochem. Sci.* **12,** 390–394

Supplementary Material to

Inulin-^{125}I-Tyramine, an Improved Residualizing Label for Studies on Sites of Catabolism of Circulating Proteins

by Janet L. Maxwell, John W. Baynes and Suzanne R. Thorpe

EXPERIMENTAL PROCEDURES

Materials: $NaBH_3CN$, tyramine, inulin (dahlia tuber, M_r~5000), bovine serum albumin (BSA) and insolubilized neuraminidase were purchased from Sigma Chemical Co. Carrier-free $Na^{125}I$ (*I) (100 mCi/ml 0.1 N NaOH) was obtained from Amersham and NaB^3H_4 (532 mCi/mmol) from NEN Research Products. Cyanuric chloride (CyCl) (Aldrich) was recrystallized from benzene and stored at -20° C. DLT was synthesized and iodinated as described previously (3). Rat serum albumin (RSA) was purified from fresh serum by affinity, ion exchange and gel exclusion chromatography, and iodinated using Iodogen (Pierce) as described previously (7). Fetuin (FET) was obtained from Gibco and a monomer fraction isolated by chromatography on Sephacryl S-200 (Pharmacia) in Dulbecco's (12) phosphate buffered saline (PBS) (137 mM NaCl, 2.7 mM KCl, 8.1 mM Na_2HPO_4, 1.7 mM KH_2PO_4, pH 7.4). The final RSA and FET preparations were >95% homogeneous by sodium dodecylsulfate polyacrylamide gel electrophoresis (SDS-PAGE) under reducing conditions (13).

Synthesis and Purification of InTn: The scheme in Fig. 1 shows our route to synthesis and iodination of InTn and coupling of *I-InTn to protein. Inulin is generally described as a non-reducing polysaccharide of fructose linked to a terminal sucrose residue, however most commercial preparations contain a fraction of incomplete chains with a reducing fructose terminus (14). Some enrichment for reducing inulin was obtained by fractionating inulin on Sephadex G-50 and pooling the fractions with highest ratio of reducing sugar, measured by the bicinchoninic acid assay (15), to total sugar, measured by the anthrone assay (16) (Fig. 2A), using fructose as standard in both assays. The synthesis of InTn was carried with the enriched inulin pool (Fig. 2A), using an adaptation of the procedure of Raja et al. (17) for reductive amination of hyaluronic acid with aliphatic amines. This procedure involves reduction of the terminal sugar unit to an alditol, followed by limited oxidation with periodate to generate a reactive aldehyde terminus, and reductive amination of the polysaccharide with the amine.

Reagent ratios in subsequent reactions are based on the content of reducing ends in the fractionated inulin preparation. For a typical InTn preparation, inulin (12 mg total inulin/ml, 1.16 umole reducing sugar/ml) was dissolved in 0.1 M potassium borate, pH 8.3; a 100-fold excess of solid $NaBH_4$ was added and the solution stirred for 4 h at room temperature. The reaction was quenched with 50 ul acetone, and 4 volumes of ice cold ethanol were added (final concentration 80%) to precipitate inulin and its derivatives. The solution was centrifuged in an IEC Centra 7R centrifuge at 4°C for 10 min at 2500 rpm, the supernatant discarded and residual ethanol removed from the precipitate under a stream of nitrogen. The pellet was redissolved in 1.25 ml 30 mM imidazole, pH 6.5, a 4-fold excess of solid $NaIO_4$ added, and the mixture stirred at room temperature for 1 hr when all the periodate had been consumed, based on assay for free periodate (18). The periodate treated inulin was recovered following ethanol precipitation as above, immediately redissolved in 1.25 ml 0.1 M potassium borate, pH 7.25, and an 8-fold excess of solid tyramine added and the solution stirred at room temperature for 15 min to allow Schiff-base formation; a 100-fold excess of $NaBH_3CN$ was then added and reductive amination carried out overnight at room temperature with stirring. Solid $NaBH_4$ (25-fold excess) was then added and the mixture let stand for another hour in order to reduce any remaining oxidized groups. Inulin and derivatives were precipitated with ethanol and the pellet dissolved in 0.1 M NaCl and chromatographed on Sephadex G-50 (Fig. 2B). Fractions containing InTn (Fig. 2B, fractions 25-33) were pooled, concentrated and desalted on Sephadex G-25 in H_2O. The desalting step also removed any residual free tyramine and yielded a final InTn preparation containing ~0.2 mol tyramine/mol inulin.

Labeling of Inulin and InTn. $[^3H]$-inulin was prepared by reduction of fractionated inulin with a 10-fold excess of NaB^3H_4, as described above. InTn was iodinated using methods described previously for the iodination of DLT and other residualizing labels (3). Typically, InTn (10 nmol based on tyramine absorbance at 220 nm) in 25 ul 0.5 M potassium phosphate, pH 7.7, was placed in a 0.5 ml polypropylene centrifuge tube coated with 20 ug dried Iodogen. Na*I, 1 mCi in 10 ul 0.1 N NaOH, was added and the iodination carried out at room temperature for 20-30 min. The *I-InTn was isolated by centrifugal chromatography on a 1 ml Sephadex G-25 (Pharmacia) column in water (2 min in an IEC Model HN centrifuge at 900 rpm). When an aliquot of the *I-InTn was added to carrier inulin (25 mg/ml), >85% of the radioactivity was precipitable by 80% ethanol. The efficiency of iodination was about 30%. As shown in Fig. 2C, *I-InTn radioactivity co-chromatographed with total carbohydrate (added carrier) on Sephadex G-50.

Coupling of *I-InTn to Protein. The procedure for the coupling of tyramine derivatives to protein using CyCl is similar to that described previously (3). For a typical labeling, *I-InTn, 10 nmol in 35 ul 0.15 M potassium phosphate, pH 7.7, was placed in a 0.5 ml polypropylene tube and activated by addition of an equimolar amount of CyCl in 4 ul of acetone. After 30 sec, protein, 2 mg (30-40 nmol of RSA or FET, respectively) in 50-200 ul PBS was added with vortexing. To estimate the efficiency of coupling to protein, a 1 ul aliquot of the reaction mixture was removed after 5-10 min and added to carrier protein, 2 mg bovine serum albumin (BSA) in 300 ul H_2O, then precipitated with an equal volume of 40% trichloroacetic acid (TCA). Efficiency of coupling was 50-70% for

the various proteins tested. The *I-InTn-protein was separated from free *I-InTn following dialysis and chromatography on Sephacryl S-200 as described previously (3). *I-InTn-asialofetuin (*I-InTn-ASF) was prepared by treatment of *I-InTn-FET (10 mg/ml 0.1 M Na acetate, pH 5.2) with one-half unit of insolubilized neuraminidase for 4 h at 25 C. The desialylated protein was re-isolated by chromatography on Sephacryl S-200 in PBS. No protein polymers were detected in these labeling experiments since >95% of applied radioactivity was recovered in a single protein band on SDS-PAGE.

In Vivo Experiments. Experiments were carried out in male and female Sprague-Dawley rats, 130-220 g. Methods for animal care and maintenance, injection of proteins, and measurement of plasma and whole body radioactivity have been described previously (3,7). Unless otherwise indicated, all data points for plasma and whole body clearance curves are averages for at least 3 animals and absence of error bars indicates that the coefficient of variation was ≤5%. Plasma and whole body half-lives were estimated by linear regression analysis. Total and acid soluble radioactivity in tissues were distinguished by precipitation with 20% TCA as described previously (3,7). In control experiment *I-InTn, *I-InTn-FET or *I-InTn-RSA was added to nonradioactive liver or skin, and processed for determination of acid soluble radioactivity. Recoveries of soluble radioactivity were 94-97% for *I-InTn, and 3-9% for *I-InTn-FET and *I-InTn-RSA. Subcellular fractionation of liver by differential centrifugation was performed according to Gregoriadis and Sourkes (19), using beta-N-acetylhexosaminidase as a lysosomal marker enzyme

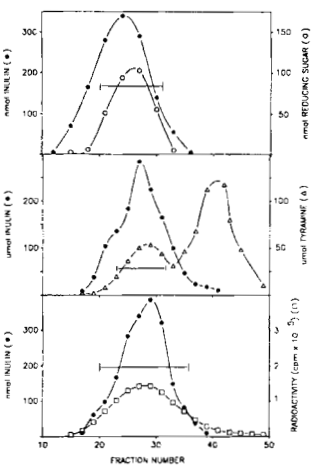

Figure 2. Chromatographic characterization of inulin and derivatives.
2A (top): Chromatography of natural inulin. Inulin (20 mg) was dissolved in 2 ml 0.2 M NaCl and chromatographed on a Sephadex G-50 column (1.5 x 47 cm) in 0.2 M NaCl. Fractions, 2 ml, were collected and assayed for total (●) and reducing (○) sugar as described in Materials and Methods. Total sugar, measured as fructose, was converted to nmol inulin assuming M_r = 5,000. Fractions 24-33 (bracketed in figure) were pooled for preparation of InTn.

2B (middle): Chromatography of an InTn reaction mixture. After coupling of tyramine to inulin aldehyde, the ethanol precipitate was dissolved in 0.2 M NaCl and chromatographed as above. Fractions were assayed for total carbohydrate (○) and tyramine by absorbance at 220 nm (△). Fractions 19-27 (bracketed in figure) were pooled for preparation of *I-InTn.
2C (bottom): Chromatographic profile of *I-InTn, prepared as described in Materials and Methods. Unlabeled carrier inulin was added to obtain the total carbohydrate profile (●).

RESULTS

Chemistry of Coupling *I-InTn to Protein. One concern about coupling residualizing labels to proteins is that the modification of the protein may affect the biological properties of the protein. To minimize structural alterations in the protein the labeling reaction is normally designed to yield <1 mol label/mol protein in order to decrease the probability of modifying the same protein molecule twice. With the InTn label there was also the possibility that the protein could be modified by the 80% inulin carrier in the *I-InTn preparation. This seemed unlikely because of the much higher pH required for reaction between CyCl and carbohydrates (22), but the inertness of the carrier inulin was also confirmed experimentally. As shown in Table I, CyCl coupling of *I-InTn to BSA proceeded with an efficiency of 70%, compared to <1% for [^{3}H]inulin or in control experiments without CyCl. The results are consistent with our previous work indicating that CyCl couples *I-DLT to protein via the tyramine moiety (3).

Table I

Efficiency of coupling of [^{3}H]Inulin and *I-InTn to protein

Compound[a]	Acid-Precipitable Radioactivity[b] Experimental (%)	Control[c] (%)
[^{3}H]Inulin	<1	<1
*I-Inulin-tyramine	70	<1

[a] Prepared as described in Materials and Methods. Specific activities were 7.1 x 10^3 cpm/nmol [^{3}H]inulin and 29 x 10^6 cpm/nmol *I-InTn. The specific radioactivity of *I-InTn is based on its tyramine content, i.e., 0.2 nmol tyramine/nmol total inulin, thus 10 nmol *I-InTn contains the equivalent of 50 nmol total inulin.
[b] Radioactive compounds (50 nmol [^{3}H]inulin and 10 nmol *I-InTn) were activated with 10 nmol CyCl, reacted with BSA (2 mg, 30 nmol in 200 ul phosphate buffer) and aliquots removed and assayed for acid precipitable radioactivity as described in Materials and Methods.
[c] CyCl was omitted from control experiments.

Preliminary Evaluation of the *I-InTn Label. ASF is used as a model protein for evaluating residualizing labels because its kinetics of clearance from the circulation, its mechanism of uptake by hepatocytes and eventual degradation in lysosomes are well-characterized (23). As shown in Fig 3A, *I-InTn-ASF was cleared from the rat circulation with a half-life of less than 1 min. These kinetics were essentially identical to those for clearance of *I-ASF (3). Co-injection of an excess of unlabeled ASF increased the half-life of *I-InTn-ASF to greater than 0.5 h, consistent with saturation of the hepatocyte receptor for galactose-terminal glycoproteins and indicative that attachment of *I-InTn did not interfere with clearance of ASF by this receptor-mediated pathway. In the absence of competitor, more than 90% of injected radioactivity from *I-InTn-ASF was recovered in liver at 15 min after injection.

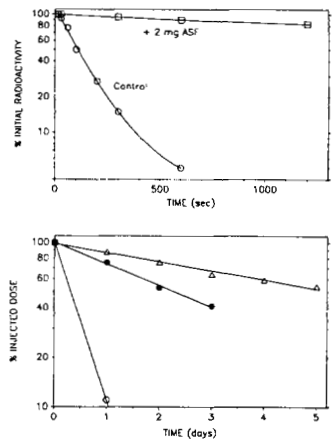

Figure 3. Kinetics of plasma and whole body clearance of radioactivity following injection of labeled ASF.
3A (top): Plasma clearance of *I-InTn-ASF and competition by co-injection of 2 mg unlabeled ASF. Animals were injected with 5 x 10^6 cpm (~50ug) of labeled protein. Data points are average values for 2 animals in each experiment.
3B (bottom): Kinetics of whole body clearance of radioactivity from ASF labeled with *I (○), *I-DLT (●) or *I-InTn (△). For each experiment animals were injected with 2-3 x 10^6 cpm (<50 ug) labeled protein.

In order to trace the disposition of *I-InTn metabolites in liver, animals were injected with *I-InTn-ASF and sacrificed at 1 h, 1, 3 and 5 d. In all cases >90% of hepatic radioactivity was in acid soluble form. In addition, 92-95% of radioactivity remaining in the body was recovered in the liver at all times; stomach, intestines their contents accounted for a maximum of 2-3% of recovered radioactivity, indicating minimal redistribution of the label into other tissues. Animals were also sacrificed at 1 h, 1 and 3 d after injection, and livers removed and fractionated into nuclear, mitochondrial-lysosomal and supernatant fractions (19). The recovery of radioactivity in these fractions corresponded to recovery of the lysosomal marker enzyme, beta-N-acetylhexosaminidase. In all cases, <10% of radioactivity and enzyme activity were found in the post-lysosomal supernatant fraction, whereas when intact *I-InTn-ASF was homogenized with liver and fractionated, 96% of the radioactivity, but only 12% of beta-N-acetylhexosaminidase activity, was recovered in the supernatant. In general, the results of these experiments with *I-InTn-ASF agreed closely with results obtained previously with other residualizing labels, such as [^{3}H]raffinose (2) and *I-DLT (3). Thus, despite its size, the attachment of *I-InTn did not detectably affect the uptake, compartmentation or catabolism of ASF in liver.

Since *I-InTn-ASF was degraded to acid soluble products in liver within 1 h, the loss of radioactivity from the whole body was used as a measure of the efficiency of residualization of the label. A comparison of the whole body kinetics of clearance of *I-ASF, *I-DLT-ASF and *I-InTn-ASF is shown in Fig. 3B. The residualization of the InTn label shows about a 2-fold improvement over that of DLT, with half-lives of 2.3 and 5.1 d for the *I-DLT and *I-InTn degradation products, respectively. The improvement in residualization with *I-InTn is consistent with the relationship between molecular weight and efficiency of residualization observed in our previous studies (3).

Studies with Long-lived Proteins. The *I-InTn label was next applied to studies on the catabolism of native fetuin. Fig. 4 shows that the whole body half-life of radioactivity from *I-FET is about 1 d, which is equal to its plasma half-life in the rat (24), while the whole body half-lives were 3-3.5 and 5-6 d for *I-DLT-FET and *I-InTn-FET, respectively, in several experiments. The tissue distribution of radioactivity was determined, as described in Materials and Methods, at 2 d (2 half-lives) after injection of *I-DLT-FET and *I-InTn-FET. The overall distribution of radioactivity was similar in both cases (data not shown), with the majority of degradation products being recovered in muscle and skin, in agreement with earlier studies using the residualizing label, [^{3}H]raffinose (24).

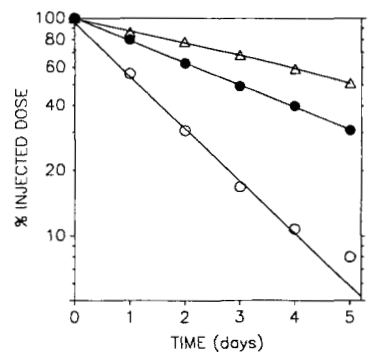

Figure 4. Kinetics of whole body clearance of radioactivity from fetuin labeled with *I (○), *I-DLT (●) or *I-InTn (△). Animals were injected with 2.5 x 10^6 cpm (25-50 ug) of labeled protein.

The tissue distribution of radioactivity at 4 d after injection of *I-InTn-RSA, shown in Table II, confirms previous evidence using *I-DLT-RSA that catabolism of RSA takes place primarily in muscle and skin (7).

Table II

Recovery of radioactivity and distribution of degradation products in tissues 4 days after injection of *I-InTn-RSA in rats[a]

Tissue	%cpm recovered in body[b]	% acid-soluble radioactivity	%protein catabolized[c]
Skin	37.8 ± 2.9	67.8 ± 4.9	25.6
Muscle	30.9 ± 1.7	51.9 ± 4.8	16.0
Fat	9.1 ± 2.0	70.4 ± 6.6	6.4
Liver	7.5 ± 0.2	74.9 ± 1.4	5.6
Kidney	2.4 ± 0.2	75.7 ± 0.9	1.8
Spleen	0.8 ± 0.2	78.4 ± 0.7	0.6
Blood	9.8 ± 1.5	<1	

[a] Animals were injected with 12 x 10^6 cpm (~100 ug) *I-InTn-RSA. Total and acid soluble radioactivity in tissues were measured as described in Materials and Methods.

[b] Data are expressed as means and standard deviations for three animals. Recovery of radioactivity in the body at 4 days was 73 ± 1 % of injected dose. The sum of radioactivity recovered in tissues and excreta accounted for 91 ± 5 % of injected dose. Less than 7% of total radioactivity was recovered in toto in heart, lung, thymus, thyroid, bone, and stomach and intestine and their contents.

[c] Percent protein catabolized was determined by multiplying the average % recovered dose (Column 2) by the average % acid-soluble radioactivity (Column 3) for each tissue.

Kinetic Modeling of Plasma Protein Catabolism. The model shown in Fig. 6 was chosen as the simplest three compartment model for describing the pathway of catabolism of plasma proteins. This model treats all extracellular protein as a single pool and assumes that the distribution of the protein between vascular and extravascular compartments exerts an insignificant effect on its fractional catabolic rate (FCR). This assumption is supported by the observation that the kinetics of whole-body elimination of radioactivity from *I-FET and *I-RSA (Figures 4 and 5B) are linear from time of injection and extrapolate to essentially 100% of injected dose at zero time. The FCR (k_1) for these proteins can be estimated from the slope of either the whole body clearance curve for *I-labeled protein or the linear phase of the plasma clearance curves using any of the labels; the two methods yield identical results, i.e., the slopes are identical within experimental error (cf. Fig. 5).

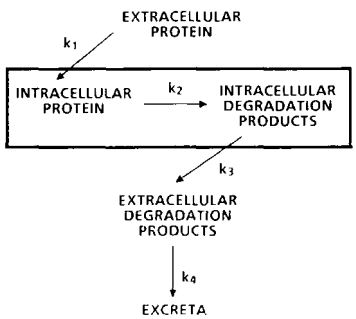

Figure 6. Basic kinetic model for catabolism of plasma proteins and disposition of degradation products.

The differential equations used in the SCoP program to define the model in Fig. 6 are straightforward:

$$(1)\quad d(PL)/dt = -k_1*(PL),$$

$$(2)\quad dC/dt = k_1*(PL) - k_3*C, \text{ and}$$

$$(3)\quad dE/dt = k_3*C;$$

where PL = intact tracer in the extracellular (plasma + lymph) space,

C = labeled catabolites in the intracellular compartment, and

E = labeled catabolites in excreta.

The constants, k_2 and k_4, are not used in the calculations for the model since, based on experiments with ASF (Fig. 3), the rates of degradation of endocytosed protein and release of exocytosed degradation products from the body are considered rapid and non-rate-limiting, compared to k_1 and k_3. For the purpose of illustrating the results of calculations, experimental data from Fig. 5B are replotted in Fig. 7, showing the kinetics of whole body release of degradation products from *I-DLT-RSA (Fig. 7A) and *I-InTn-RSA (Fig. 7B); the various curves represent different fits to the data using the SCoP or SCoPfit programs. The dotted curves in Fig. 7 were obtained assuming that the half-life for release of degradation products from tissues involved in RSA catabolism was identical to the half-life for release of ASF degradation products from liver. Specifically, the dotted lines were generated using the above mathematical model and experimentally determined k_1 value of 0.31 d^{-1} as the FCR for RSA (Fig. 5), and k_3 values of 0.30 and 0.136 d^{-1}, respectively, derived from the rates of leakage of *I-DLT-ASF and *I-InTn-ASF degradation products from liver (half-lives = 2.3 and 5.1 d, respectively, as shown in Fig. 3). The dotted curve is clearly a poor fit to the actual data on rates of whole body loss of RSA degradation products. Not only does the theoretical curve consistently overshoot the actual data points, but a more fundamental error is apparent insofar as the shape of the curves does not fit the actual trend in the data. Similar results (graphs not shown) were obtained with data on whole body clearance of *I-DLT-FET and *I-InTn-FET, using a k_1 value of 0.59, estimated from the actual half-life of *I-FET, as shown in Fig. 4.

As an alternative approach to fitting the data, it was accepted that release of ASF degradation products from liver might not be a good model for predicting the half-life of degradation products in peripheral tissues. Thus, the SCoPfit program was used to obtained optimized values of k_1 and k_3. The FCR for RSA (k_1) was assigned an initial value of 0.31 d^{-1}, with a range of 0.31-0.39 d^{-1}, i.e., a half-life of 1.8-2.2 d, the observed range for the half-life of RSA in our laboratory (5,7,25 and Fig. 5). Initial values chosen for k_3 were 0.30 and 0.136 d^{-1} for *I-DLT and *I-InTn, respectively, estimated as above from studies with *I-DLT-ASF and *I-InTn-ASF (Fig. 3); the allowed range for k_3 was 0.01-0.99 d^{-1}. The dashed lines in Fig. 7 show the calculated best fit to the data, obtained using the Runge-Kutta integrator routine in the SCoPfit program. Both of these lines also reveal a systematic deviation from the experimental data, consistently overshooting the experimental data points at early times and undershooting at later times. As in the previous analysis using SCoP, similar discrepancies and systematic errors were obtained on optimizations with data from experiments with *I-DLT-FET and *I-InTn-FET (graphs not shown). The resulting kinetic constants for the optimizations with both the RSA and FET data are summarized in Table III (Original Model). In addition to the poor fit to the data, the optimized values of k_3 are of concern since the corresponding half-lives for loss of *I-DLT and *I-InTn degradation products from the body (0.9-1.0 and 2.2-2.6 d, respectively) are short, compared to observed differences in residualization of degradation products from *I-, *I-DLT- and *I-InTn-labeled proteins (Fig. 4 and 5B).

Table III

Summary of kinetic constants determined by optimization programs

Protein	Label	Kinetic Constants or Half-Lives: Original Model[a] k_1[b] (d^{-1})	Original Model[a] k_3[c] (d^{-1})	Original Model[a] $t_{1/2}$[c] (days)	Compartmental Model[a] k_{1s}[d] (d^{-1})	Compartmental Model[a] F_s[e] (%)	Compartmental Model[a] k_{3s}[f] (d^{-1})	Compartmental Model[a] $t_{1/2}$[f] (days)
ASF	*I-DLT	<0.01	0.31	2.3	-	-	-	-
	*I-InTn	<0.01	0.136	5.1	-	-	-	-
FET	*I-DLT	0.58	0.74	0.94	0.31	53	0.29	2.5
	*I-InTn	0.58	0.32	2.2	0.43	73	0.17	4.3
RSA	*I-DLT	0.31	0.70	1.0	0.12	38	0.23	3.0
	*I-InTn	0.31	0.27	2.6	0.24	77	0.16	4.3

[a] Original Model is described in Fig. 6. Compartmental Model, described in text, allows for partitioning of degradation products into fast and slow release compartments.

[b] The constant, k_1, is equivalent to the FCR of the protein.

[c] The constant, k_3, and the corresponding half-life ($t_{1/2}$) refer to the kinetics of release of degradation products from cells, as determined experimentally for ASF and by SCoPfit for FET and RSA.

[d] The constant, k_{1s}, refers to the rate of uptake of protein into the slow release compartment; k_{1s} is one component of the total FCR.

[e] F_s represents the percent of total protein catabolism shunted into the slow release compartment. It is determined as: $F_s = k_{1s}/k_{1t}$.

[f] The constant, k_{3s}, and the corresponding half-life refer to the kinetics of release of degradation products from the slow-release compartment, as determined by SCoPfit optimization.

Overall, the fitted curves generated in the above analyses do not correlate well with experimental data, suggesting that the three-compartment sequential model in Fig. 6 is not an adequate representation of the biological process. Admittedly, there are a number of simplifying assumptions involved in the model, but it is disconcerting that even the curve shapes are inconsistent with the trends in the data. Thus, while the kinetics of release of degradation products from the body are pseudo-first order in "% dose remaining" (Figs. 4 and 5B), the sequential model predicts some initial period during which radioactive degradation products should accumulate in the intracellular compartment. Thus, as observed with both the dotted and dashed lines obtained in the previous analyses, there should be a lag phase in the release of degradation products from the body while. In fact, however, the data for *I-DLT-RSA and *I-DLT-FET extrapolate nearly linearly (on a semi-log plot) to 100% of dose at zero time, while there is only a slight indication of a lag-phase for release of *I-InTn-FET and *I-InTn-RSA products (Figs. 4, 5B and 7). One possible explanation for this discrepancy is that residualizing labels are not retained efficiently by all cell types, and that some cells may release degradation products with minimal kinetic delay. This was considered unlikely, however, because non-degradable compounds are known to residualize well in all cell types which have been studied thus far in vivo and in vitro. Relevant studies in vivo include those demonstrating retention of residualizing labels in hepatocytes using ASF as carrier protein (2,3,24 and Fig 4), hepatic non-parenchymal cells using RNase B and heat-denatured albumin (2,24), skin and muscle fibroblasts using RSA (7) and aortic endothelial using lipoproteins (26). In addition, studies in vitro have shown that residualizing labels are retained efficiently in fibroblasts (8,10) and in cardiac endothelial cells (unpublished observations). Finally, numerous studies have shown that non-degradable compounds, including sucrose (27,28), cellobiose and ficoll (27) and poly-D-amino acids (29) accumulate in macrophage lysosomes in vitro. The widespread pathology associated with various lysosomal storage diseases also suggests that at least temporary accumulation of non-degradable materials is characteristic of cellular metabolism.

A possible explanation for poor fit between between model and data was suggested by recent studies of Buktenica et al. (30) who have proposed that proteins taken into cells by fluid-phase endocytosis, along with their degradation products, may be excreted from cells by two distinct pathways, i.e. from rapid and slow release compartments. In their studies they demonstrated that a fraction of degradation products from *I-labeled proteins were released from cells (mouse peritoneal macrophages and baby hamster kidney fibroblasts) with a half-life of 5-10 min, while another fraction was apparently trapped in a lysosomal compartment and released with a half-life of 1-2 d in vitro. These observations suggested to us that degradation products containing residualizing labels might also be partitioned in cells in vivo. One fraction might be released rapidly, explaining the absence of a lag phase in release of degradation products from the body, and another fraction retained and released slowly from the lysosomal compartment. It can then be postulated that both of these routes are accessible to all endocytosed proteins, and that differential residualization would result from differences in partitioning of the degradation products between the two pathways.

As a test of this hypothesis, the original model (Fig. 6) was modified to a compartmental model which allowed for rapid release of a fraction of degradation products from cells. The equations for the model for RSA were modified as follows:

$$(1)\quad d(PL)/dt = -k_{1t}*(PL),$$

$$(2)\quad dC/dt = k_{1s}*(PL) - k_{3s}*C, \text{ and}$$

$$(3)\quad dE/dt = k_{3s}*C + k_{1f}*(PL);$$

where k_{1t} is the total FCR for RSA (0.31 d^{-1}), k_{1s} and k_{1f} represent the fraction of total FCR occurring via the slow- and fast-release compartments, respectively, and k_{3s} is the rate constant for release of RSA degradation products from the slow-release compartment. The range for k_{1s} was limited to 0.01-0.31 d^{-1}, i.e., $\sim k_{1t}$, where $k_{1t} = k_{1s} + k_{1f}$, and the range for k_{3s} was 0.01-0.99 d^{-1}. The SCoPfit program was used to optimize k_{1s} and k_{3s} to fit experimental data, and, as shown by the solid lines in Figures 7A and 7B, excellent fits were obtained for data from experiments with both *I-DLT-RSA and *I-InTn-RSA. Equally good fits (graphs not shown) were obtained for the experiments with *I-DLT-FET and *I-InTn-FET (Fig. 4), substituting the constant, 0.59 d^{-1} for 0.31 d^{-1} in the above equations. The estimated percent of degradation products released via the slow-release compartment and the kinetic constants, k_{3s}, and corresponding half-lives for retention of residualizing labels obtained from the several experiments were internally consistent and reasonable. Thus, the the fraction of degradation products shunted into the slow release compartment (F_s, Table III, Col. 7) increases from 38-53% for *I-DLT-labeled FET and RSA to 73-77% for the *I-InTn-labeled proteins, consistent with increased efficiency of residualization of *I-InTn-labeled degradation products. In addition, the values of k_{3s} estimated with FET and RSA for *I-DLT and *I-InTn degradation products are 2.5-3.0 and 4.3 d, respectively (Table III, Col. 9) and are in reasonable agreement with the 2.3 and 5.1 d half-lives observed for ASF degradation products in liver (Table III, Col. 4, and Fig. 3). While this model represents all cells involved in the catabolism of RSA or FET as a single compartment and assumes that the distribution of degradation products between slow and fast release compartments and their rates of transport through the cell are identical for all cell types, there is not a sufficient amount of experimental data with various proteins and labels to justify a more sophisticated treatment at this time. However, the internal consistency and reasonableness of the kinetic constants obtained from the optimization, as well as the quality of the fit to experimental data for both FET and RSA, lend some support to the compartmental model and justify continued experimentation to test the model in vivo and in simpler model systems in vitro.